Electronic Transactions on Numerical Analysis.
Volume 55, pp. 706–725, 2022.

ISSN 1068–9613.
DOI: 10.1553/etna_vol55s706

ETNA
Kent State University and
Johann Radon Institute (RICAM)

A POSTERIORI ERROR ESTIMATES FOR STABILISED MIXED FINITE ELEMENT METHODS FOR A NONLINEAR ELLIPTIC PROBLEM*

MARíA GONZÁLEZ† AND HIRAM VARELA†

Abstract. In this paper we propose new adaptive stabilised mixed finite element methods for a nonlinear elliptic boundary value problem of second order in divergence form that appears, among other applications, in magnetostatics. The method is based on a three-field formulation that is augmented with suitable residual least-squares terms arising from the constitutive and equilibrium equations and from the equation that defines the gradient as an additional unknown. We show that the resulting scheme is well posed and obtain optimal error estimates. We also develop an a posteriori error analysis of residual type and derive a simple a posteriori error indicator which is reliable and locally efficient. Finally, we include several numerical experiments that confirm the theoretical results.

Key words. nonlinear boundary value problem, mixed finite element, stabilisation, a posteriori error estimates, magnetostatics

AMS subject classifications. 65N12, 65N15, 65N30, 65N50

1. Introduction.

In this paper we consider a nonlinear elliptic problem of second order in divergence form. This kind of problems appear in the modeling of a wide range of phenomena, such as steady heat conduction, magnetostatics, or the minimal surface problem, among others. Mixed formulations for this kind of problems are sometimes treated through the inversion of the constitutive equation using the implicit function theorem (see, for instance, [17, 18, 15]). When the constitutive equation is not explicitly invertible, one can introduce additional unknowns, like in the expanded mixed finite element method [7, 8] and the dual-dual formulation from [12].

In this work we consider as starting point the variational formulation proposed in [12]. There, two compatibility (inf-sup) conditions between the discrete spaces are required in order to ensure that the corresponding Galerkin scheme is well-posed. Augmented formulations based on adding residual terms of least-squares type for the variational formulation (see, for instance, [16, 4] and the references therein) will allow us to avoid this requirement.

In order to improve the convergence behaviour of the discrete solution, one can apply adaptive methods based on a posteriori error estimates. In this respect, Araya et al. [2] proposed a reliable a posteriori error estimate that depends on the solution of a local linear boundary value problem for the dual-dual method presented in [12]. Moreover, for specific finite element subspaces of Raviart-Thomas type, the authors provide a fully explicit a posteriori error estimate that uses some reasonable approximation of the exact finite element solution. More recently, Garralda et al. [11] derived reliable and efficient a posteriori error estimators for the same Galerkin scheme.

The aim of the present paper is to introduce and analyse an adaptive augmented dual-mixed method for the nonlinear elliptic problem considered in [12]. We show that the new continuous and discrete augmented variational problems are well posed and that a Céa-type estimate holds. We also derive optimal rates of convergence. We obtain a simple a posteriori error indicator which is reliable and locally efficient and show some numerical experiments that support the theoretical results.

The paper is organised as follows. The model problem is described in Section 2. The new augmented variational formulation is presented and analysed in Section 3. The associated

*Received August 24, 2021. Accepted June 17, 2022. Published online on September 1, 2022. Recommended by Simona Perotto.

†Departamento de Matemáticas and CITIC, Universidade da Coruña, Campus de Elviña s/n, 15071, A Coruña, Spain ({maria.gonzalez.taboada,hiram.varela}@udc.es).

ETNA
Kent State University and
Johann Radon Institute (RICAM)

discrete problem is discussed in Section 4. Then an a posteriori error analysis of residual type is developed in Section 5. Finally, several numerical experiments are presented in Section 6, and conclusions are drawn in Section 7.

In what follows, we employ the usual notations for Lebesgue and Sobolev spaces. Moreover, C, with or without subscripts, denotes a generic constant independent of the discretisation parameter that may take different values at different occurrences.

2. Model problem. We consider a bounded and simply connected domain $\Omega \subset \mathbb{R}^2$ with a Lipschitz continuous boundary Γ. Given the functions $f \in L^2(\Omega)$, $g \in H^{1/2}(\Gamma)$, and $k\colon \Omega \times [0,+\infty) \to \mathbb{R}$, the problem reads:

Find $u \in H^1(\Omega)$ such that

$$\begin{cases} -\nabla \cdot (k(\cdot,|\nabla u|)\nabla u) = f & \text{in } \Omega\,, \\ u = g & \text{on } \Gamma, \end{cases} \tag{2.1}$$

where $|\cdot|$ denotes the Euclidean norm. This kind of problem appears, for instance, in steady heat conduction and magnetostatics (see [22] and the references therein).

In what follows, we assume that $k \in \mathcal{C}^1(\Omega \times [0,+\infty))$ and that there exists positive constants k_1 and k_2 such that

$$k_1 \le k(\mathbf{x},s) + s\frac{\partial k}{\partial s}(\mathbf{x},s) \le k_2\,, \qquad \forall\,(\mathbf{x},s) \in \Omega \times [0,+\infty)\,. \tag{2.2}$$

We remark that by integrating (2.2) in $[0,t]$ for $t > 0$, we obtain

$$k_1 \le k(\mathbf{x},s) \le k_2\,, \qquad \forall\,(\mathbf{x},s) \in \Omega \times [0,+\infty)\,.$$

Some examples of functions k satisfying the assumption (2.2) can be found, for example, in [22].

In the next lemma we collect some well-known results that will be used in the following.

LEMMA 2.1. *Assume that k satisfies (2.2). Then there exists positive constants C_0, C_1, and α such that for all $\mathbf{t}$, $\mathbf{s}$, $\mathbf{z} \in [L^2(\Omega)]^2$,*

$$\left| \int_\Omega (k(\cdot,|\mathbf{t}|)\mathbf{t} - k(\cdot,|\mathbf{s}|)\mathbf{s}) \cdot \mathbf{z} \right| \le C_0 \,\|\mathbf{t}-\mathbf{s}\|_{[L^2(\Omega)]^2} \|\mathbf{z}\|_{[L^2(\Omega)]^2}\,, \tag{2.3}$$

$$\left| \int_\Omega k(\cdot,|\mathbf{t}|)\mathbf{t} \cdot \mathbf{z} \right| \le C_1(1 + \|\mathbf{t}\|_{[L^2(\Omega)]^2}) \|\mathbf{z}\|_{[L^2(\Omega)]^2}\,, \tag{2.4}$$

$$\int_\Omega (k(\cdot,|\mathbf{t}|)\mathbf{t} - k(\cdot,|\mathbf{s}|)\mathbf{s}) \cdot (\mathbf{t}-\mathbf{s}) \ge \alpha \,\|\mathbf{t}-\mathbf{s}\|^2_{[L^2(\Omega)]^2}\,. \tag{2.5}$$

Proof. See, for instance, [22]. ∎

In the next section we recall the dual-dual mixed variational formulation studied in [12] and analyse a new augmented variational formulation for problem (2.1).

3. Augmented dual-mixed variational formulation. We follow [2] (see also [12]) and introduce $\mathbf{t} = \nabla u$ and $\boldsymbol{\sigma} = k(\cdot,|\mathbf{t}|)\mathbf{t}$ in Ω as further unknowns. Then the first equation of problem (2.1) can be rewritten as

$$-\nabla \cdot \boldsymbol{\sigma} = f, \qquad \text{in } \Omega\,.$$

We denote by $H(\nabla\cdot,\Omega) := \{\boldsymbol{\tau} \in [L^2(\Omega)]^2 \,:\, \nabla\cdot\boldsymbol{\tau} \in L^2(\Omega)\}$ and consider the dual-mixed variational formulation introduced in [2, 12]:

ETNA
Kent State University and
Johann Radon Institute (RICAM)

Find $(\mathbf{t},\boldsymbol{\sigma},u)\in[L^2(\Omega)]^2\times H(\nabla\cdot,\Omega)\times L^2(\Omega)$ such that

$$\left\{\begin{array}{l} \displaystyle\int_\Omega k(\cdot,|\mathbf{t}|)\mathbf{t}\cdot\mathbf{s}-\int_\Omega\boldsymbol{\sigma}\cdot\mathbf{s}=0,\\ \displaystyle-\int_\Omega\boldsymbol{\tau}\cdot\mathbf{t}-\int_\Omega u\,\nabla\cdot\boldsymbol{\tau}=-\langle\boldsymbol{\tau}\cdot\mathbf{n},g\rangle,\\ \displaystyle-\int_\Omega v\,\nabla\cdot\boldsymbol{\sigma}=\int_\Omega f\,v, \end{array}\right. \tag{3.1}$$

for all $(\mathbf{s},\boldsymbol{\tau},v)\in[L^2(\Omega)]^2\times H(\nabla\cdot,\Omega)\times L^2(\Omega)$, where $\mathbf{n}$ is the unit outward normal to Γ and $\langle\cdot,\cdot\rangle$ denotes the duality pairing between $H^{-1/2}(\Gamma)$ and $H^{1/2}(\Gamma)$ with respect to the $L^2(\Gamma)$-inner product. We remark that the variational formulation (3.1) has a twofold saddle point structure. The corresponding solvability result can be found in [12, Theorem 4.1].

Now, let us denote $V=H^1_0(\Omega)$ if $g=0$ or $V=H^1(\Omega)$ if $g\neq 0$. Then we assume that the solution $u\in V$, and we consider the following residual identities:

$$\begin{array}{ll} \displaystyle\xi_1\int_\Omega(\boldsymbol{\sigma}-k(\cdot,|\mathbf{t}|)\mathbf{t})\cdot\boldsymbol{\tau}=0\,, & \displaystyle\xi_2\int_\Omega\nabla\cdot\boldsymbol{\sigma}\,\nabla\cdot\boldsymbol{\tau}=-\xi_2\int_\Omega f\,\nabla\cdot\boldsymbol{\tau}\,,\\ \displaystyle\xi_3\int_\Omega(\nabla u-\mathbf{t})\cdot(\nabla v+\mathbf{s})=0\,, & \displaystyle\xi_4\int_\Gamma u\,v=\xi_4\int_\Gamma g\,v\,, \end{array} \tag{3.2}$$

where ξ_1, ξ_2, and ξ_3 are positive constants and ξ_4 is a positive constant if $g\neq 0$ or $\xi_4=0$ if $g=0$.

Subtracting the second equation in (3.1) from the first one and adding the third equation and the residual identities in (3.2), we obtain the following augmented dual-mixed variational formulation of problem (2.1):

Find $(\mathbf{t},\boldsymbol{\sigma},u)\in X:=[L^2(\Omega)]^2\times H(\nabla\cdot,\Omega)\times V$ such that

$$A((\mathbf{t},\boldsymbol{\sigma},u),(\mathbf{s},\boldsymbol{\tau},v))=F(\mathbf{s},\boldsymbol{\tau},v)\,,\qquad\forall(\mathbf{s},\boldsymbol{\tau},v)\in X\,, \tag{3.3}$$

where $A\colon X\times X\to\mathbb{R}$ is the nonlinear form defined by

$$\begin{aligned} A((\mathbf{t},\boldsymbol{\sigma},u),(\mathbf{s},\boldsymbol{\tau},v)):=&\int_\Omega k(\cdot,|\mathbf{t}|)\mathbf{t}\cdot\mathbf{s}-\int_\Omega\boldsymbol{\sigma}\cdot\mathbf{s}+\int_\Omega\boldsymbol{\tau}\cdot\mathbf{t}\\ &+\int_\Omega u\,\nabla\cdot\boldsymbol{\tau}-\int_\Omega v\,\nabla\cdot\boldsymbol{\sigma}+\xi_1\int_\Omega(\boldsymbol{\sigma}-k(\cdot,|\mathbf{t}|)\mathbf{t})\cdot\boldsymbol{\tau}\\ &+\xi_2\int_\Omega\nabla\cdot\boldsymbol{\sigma}\,\nabla\cdot\boldsymbol{\tau}+\xi_3\int_\Omega(\nabla u-\mathbf{t})\cdot(\nabla v+\mathbf{s})+\xi_4\int_\Gamma u\,v\,, \end{aligned}$$

and $F\colon X\to\mathbb{R}$ is the linear functional defined by

$$F(\mathbf{s},\boldsymbol{\tau},v):=\langle\boldsymbol{\tau}\cdot\mathbf{n},g\rangle+\int_\Omega f\,v-\xi_2\int_\Omega f\,\nabla\cdot\boldsymbol{\tau}+\xi_4\int_\Gamma g\,v\,.$$

Here we endow X with its natural norm:

$$\|(\mathbf{s},\boldsymbol{\tau},v)\|_X:=\|\mathbf{s}\|_{[L^2(\Omega)]^2}+\|\boldsymbol{\tau}\|_{H(\nabla\cdot,\Omega)}+\|v\|_{H^1(\Omega)}\,.$$

In the next two lemmas, we establish some properties of the nonlinear form $A(\cdot,\cdot)$.

ETNA
Kent State University and
Johann Radon Institute (RICAM)

LEMMA 3.1. *The nonlinear form* $A\colon X \times X \to \mathbb{R}$ *is Lipschitz continuous and bounded in* X*, that is, there exists positive constants* K *and* C_b *such that*

$$|A((\mathbf{t},\boldsymbol{\sigma},u),(\mathbf{r},\boldsymbol{\delta},w)) - A((\mathbf{s},\boldsymbol{\tau},v),(\mathbf{r},\boldsymbol{\delta},w))| \;\leq\; K\,\|(\mathbf{t},\boldsymbol{\sigma},u)-(\mathbf{s},\boldsymbol{\tau},v)\|_X\,\|(\mathbf{r},\boldsymbol{\delta},w)\|_X,$$

for all $(\mathbf{t},\boldsymbol{\sigma},u)$, $(\mathbf{s},\boldsymbol{\tau},v)$, $(\mathbf{r},\boldsymbol{\delta},w) \in X$*, and*

$$|A((\mathbf{t},\boldsymbol{\sigma},u),(\mathbf{s},\boldsymbol{\tau},v))| \;\leq\; C_b\,(1+\|(\mathbf{t},\boldsymbol{\sigma},u)\|_X)\,\|(\mathbf{s},\boldsymbol{\tau},v)\|_X,$$

for all $(\mathbf{t},\boldsymbol{\sigma},u)$, $(\mathbf{s},\boldsymbol{\tau},v) \in X$.

Proof. Let $(\mathbf{t},\boldsymbol{\sigma},u)$, $(\mathbf{s},\boldsymbol{\tau},v)$, $(\mathbf{r},\boldsymbol{\delta},w) \in X$. Then, by applying the Cauchy-Schwarz inequality and inequality (2.3) with $\mathbf{z}=\mathbf{r}$ and $\mathbf{z}=\boldsymbol{\delta}$, we obtain that A is Lipschitz continuous in X with a constant

$$K = \max(C_0, \xi_1, 4, \xi_1 C_0, \xi_2, 2\xi_3, \xi_4)\,.$$

On the other hand, using (2.4) and the Cauchy-Schwarz inequality, we have that A is bounded with

$$C_b := \max(4, \xi_1, \xi_2, 4\xi_3, \xi_1 C_1, C_1, c_t^2\xi_4)\,,$$

where c_t is the constant of the trace inequality. ∎

LEMMA 3.2. *Assume*

$$\xi_1 \in \left(0, \frac{\alpha}{2k_2^2}\right), \quad \xi_2 > 0\,, \quad \xi_3 \in \left(0, \frac{\alpha}{2}\right), \quad \text{and} \quad \xi_4 \begin{cases} = 0\,, & \text{if } g = 0\,, \\ > 0\,, & \text{if } g \neq 0\,. \end{cases} \tag{3.4}$$

Then the nonlinear form $A\colon X \times X \to \mathbb{R}$ *is strongly monotone in* X*, that is, there exists* $\tilde{\alpha} > 0$ *such that for all* $(\mathbf{t},\boldsymbol{\sigma},u)$, $(\mathbf{s},\boldsymbol{\tau},v) \in X$*,*

$$\begin{aligned} A((\mathbf{t},\boldsymbol{\sigma},u),(\mathbf{t},\boldsymbol{\sigma},u)-(\mathbf{s},\boldsymbol{\tau},v)) - A((\mathbf{s},\boldsymbol{\tau},v),(\mathbf{t},\boldsymbol{\sigma},u)-(\mathbf{s},\boldsymbol{\tau},v)) \\ \geq\; \tilde{\alpha}\,\|(\mathbf{t},\boldsymbol{\sigma},u)-(\mathbf{s},\boldsymbol{\tau},v)\|_X^2\,. \end{aligned}$$

Proof. Let $(\mathbf{t},\boldsymbol{\sigma},u)$, $(\mathbf{s},\boldsymbol{\tau},v) \in X$. Then, we use the definition of $A(\cdot,\cdot)$, (2.5), and that

$$\|k(\cdot,|\mathbf{t}|)\mathbf{t} - k(\cdot,|\mathbf{s}|)\mathbf{s}\|_{[L^2(\Omega)]^2} \;\leq\; 2k_2\,\|\mathbf{t}-\mathbf{s}\|_{[L^2(\Omega)]^2}\,. \tag{3.5}$$

We also apply Young's inequality to obtain

$$2k_2\xi_1\|\mathbf{t}-\mathbf{s}\|_{[L^2(\Omega)]^2}\|\boldsymbol{\sigma}-\boldsymbol{\tau}\|_{[L^2(\Omega)]^2} \;\leq\; \frac{\epsilon}{2}\|\mathbf{t}-\mathbf{s}\|^2_{[L^2(\Omega)]^2} + \frac{2k_2^2\xi_1^2}{\epsilon}\|\boldsymbol{\sigma}-\boldsymbol{\tau}\|^2_{[L^2(\Omega)]^2}$$

for any $\epsilon > 0$. Then, by taking $\epsilon = \alpha$, we deduce that

$$\begin{aligned} &A((\mathbf{t},\boldsymbol{\sigma},u),(\mathbf{t},\boldsymbol{\sigma},u)-(\mathbf{s},\boldsymbol{\tau},v)) - A((\mathbf{s},\boldsymbol{\tau},v),(\mathbf{t},\boldsymbol{\sigma},u)-(\mathbf{s},\boldsymbol{\tau},v)) \\ &\quad\geq\; \left(\frac{\alpha}{2}-\xi_3\right)\|\mathbf{t}-\mathbf{s}\|^2_{[L^2(\Omega)]^2} + \xi_1\left(1-\frac{2k_2^2\xi_1}{\alpha}\right)\|\boldsymbol{\sigma}-\boldsymbol{\tau}\|^2_{[L^2(\Omega)]^2} \\ &\qquad + \xi_2\,\|\nabla\cdot(\boldsymbol{\sigma}-\boldsymbol{\tau})\|^2_{L^2(\Omega)} + \xi_3\,\|\nabla(u-v)\|^2_{[L^2(\Omega)]^2} + \xi_4\,\|u-v\|^2_{L^2(\Gamma)}\,. \end{aligned}$$

So, taking the parameters ξ_1, ξ_2, ξ_3, and ξ_4 as described in (3.4), we arrive at the desired result. When $g=0$, we use the usual Poincaré inequality; when $g \neq 0$, we use the generalized Poincaré inequality:

$$\|\nabla w\|^2_{L^2(\Omega)} + \|w\|^2_{L^2(\Gamma)} \;\geq\; C_P\,\|w\|^2_{H^1(\Omega)}\,, \qquad \forall\, w \in H^1(\Omega). \qquad ∎$$

ETNA
Kent State University and
Johann Radon Institute (RICAM)

REMARK 3.3. The constant $\tilde{\alpha}$ depends on the stabilization parameters ξ_1, ξ_2, ξ_3, and ξ_4. Indeed, as can be seen from the proof of Lemma 3.2,

$$\tilde{\alpha} := \min\left(\frac{\alpha}{2} - \xi_3, \frac{\xi_1}{2}(1 - \frac{2k_2^2\xi_1}{\alpha}), \xi_2, (\xi_3 + \xi_4)C_P\right).$$

In the next lemma we establish the boundedness of the linear form $F(\cdot)$.

LEMMA 3.4. *The linear form $F\colon X \to \mathbb{R}$ is bounded: for all $(\mathbf{s}, \boldsymbol{\tau}, v) \in X$, there holds*

$$|F(\mathbf{s}, \boldsymbol{\tau}, v)| \leq (\|g\|_{H^{1/2}(\Gamma)} + \xi_4\|g\|_{L^2(\Gamma)} + (1 + \xi_2)\|f\|_{L^2(\Omega)})\|(\mathbf{s}, \boldsymbol{\tau}, v)\|_X.$$

Proof. Apply the Cauchy-Schwarz inequality and the trace inequality

$$\|\boldsymbol{\tau} \cdot \mathbf{n}\|_{H^{-1/2}(\Gamma)} \leq \|\boldsymbol{\tau}\|_{H(\nabla\cdot,\Omega)}, \qquad \forall \boldsymbol{\tau} \in H(\nabla\cdot, \Omega). \qquad \square$$

Now, we can state the main result of this section.

THEOREM 3.5. *Assume that the parameters ξ_1, ξ_2, ξ_3, and ξ_4 satisfy (3.4). Then the variational problem (3.3) has a unique solution $(\mathbf{t}, \boldsymbol{\sigma}, u) \in X$.*

Proof. The result is a consequence of Lemmas 3.1, 3.2, and 3.4. $\square$

4. Discrete problem. From now on, let us assume that Ω is a polygonal domain, let h be a positive parameter, and let $S_h \subset [L^2(\Omega)]^2$, $H_h \subset H(\nabla\cdot, \Omega)$, and $V_h \subset V$ be finite-dimensional subspaces. We define $X_h := S_h \times H_h \times V_h$. Then we consider the Galerkin scheme associated to the variational problem (3.3):

Find $(\mathbf{t}_h, \boldsymbol{\sigma}_h, u_h) \in X_h$ such that

$$A((\mathbf{t}_h, \boldsymbol{\sigma}_h, u_h), (\mathbf{s}_h, \boldsymbol{\tau}_h, v_h)) = F(\mathbf{s}_h, \boldsymbol{\tau}_h, v_h), \qquad \forall (\mathbf{s}_h, \boldsymbol{\tau}_h, v_h) \in X_h. \tag{4.1}$$

THEOREM 4.1. *Assume ξ_1, ξ_2, ξ_3, and ξ_4 satisfy (3.4). Then the discrete problem (4.1) has a unique solution $(\mathbf{t}_h, \boldsymbol{\sigma}_h, u_h) \in X_h$. Moreover, there exists $C > 0$, independent of h, such that*

$$\|(\mathbf{t}, \boldsymbol{\sigma}, u) - (\mathbf{t}_h, \boldsymbol{\sigma}_h, u_h)\|_X \leq C \inf_{(\mathbf{s}_h, \boldsymbol{\tau}_h, v_h) \in X_h} \|(\mathbf{t}, \boldsymbol{\sigma}, u) - (\mathbf{s}_h, \boldsymbol{\tau}_h, v_h)\|_X. \tag{4.2}$$

Proof. Since $X_h \subset X$, the result is a consequence of Lemmas 3.1, 3.2, and 3.4. $\square$

Let $\{\mathcal{T}_h\}_{h>0}$ be a shape-regular family of triangulations of Ω in the sense of [9] made up of triangles. For any triangle $T \in \mathcal{T}_h$ and integer $m \geq 0$, we denote by $\mathcal{P}_m(T)$ the space of polynomials of total degree at most m on T, and, given an integer $l \geq 0$, we denote by $\mathcal{RT}_l(T) := [\mathcal{P}_l(T)]^2 \oplus [\mathbf{x}]\mathcal{P}_l(T)$ the local Raviart-Thomas space of order $l + 1$ (cf. [19]), where $\mathbf{x}$ is a generic vector of $\mathbb{R}^2$. We then define the finite element spaces

$$S_h := \{\mathbf{s}_h \in [L^2(\Omega)]^2 : (\mathbf{s}_h)_{|T} \in [\mathcal{P}_m(T)]^2, \forall T \in \mathcal{T}_h\}, \tag{4.3}$$

$$H_h := \{\boldsymbol{\tau}_h \in H(\nabla\cdot, \Omega) : (\boldsymbol{\tau}_h)_{|T} \in \mathcal{RT}_l(T), \forall T \in \mathcal{T}_h\}, \tag{4.4}$$

$$V_h := \{v_h \in V \cap \mathcal{C}^0(\overline{\Omega}) : (v_h)_{|T} \in \mathcal{P}_{m+1}(T), \forall T \in \mathcal{T}_h\}. \tag{4.5}$$

ETNA
Kent State University and
Johann Radon Institute (RICAM)

We have the following rate of convergence result.

THEOREM 4.2. *Let* $(\mathbf{t},\boldsymbol{\sigma},u) \in X$ *and* $(\mathbf{t}_h,\boldsymbol{\sigma}_h,u_h) \in X_h$ *be the unique solutions to problems* (3.3) *and* (4.1)*, respectively. Assume that* $\mathbf{t} \in [H^\delta(\Omega)]^2$, $\boldsymbol{\sigma} \in [H^\delta(\Omega)]^2$ *with* $\nabla\cdot\boldsymbol{\sigma} \in H^\delta(\Omega)$ *and* $u \in H^{\delta+1}(\Omega)$*. Then there exists* $C>0$*, independent of* h*, such that*

$$\begin{aligned}&\|(\mathbf{t},\boldsymbol{\sigma},u)-(\mathbf{t}_h,\boldsymbol{\sigma}_h,u_h)\|_X\\ &\qquad\le C\,h^\beta\left(\|\mathbf{t}\|_{[H^\delta(\Omega)]^2}+\|\boldsymbol{\sigma}\|_{[H^\delta(\Omega)]^2}+\|\nabla\cdot\boldsymbol{\sigma}\|_{H^\delta(\Omega)}+\|u_h\|_{H^{\delta+1}(\Omega)}\right),\end{aligned}$$

with $\beta := \min(\delta, m+1, l+1)$.

Proof. Use the Céa estimate (4.2) and the approximation properties of the finite element subspaces (4.3)–(4.5). □

5. A posteriori error analysis. In this section, we derive a residual a posteriori error indicator for the Galerkin scheme (4.1) with the discrete spaces S_h, H_h, and V_h defined by (4.3), (4.4), and (4.5), respectively.

Let $(\mathbf{t},\boldsymbol{\sigma},u) \in X$ be the solution of the variational problem (3.3) and $(\mathbf{t}_h,\boldsymbol{\sigma}_h,u_h)$ be the solution of the discrete problem (4.1). Using the strong monotonicity of the nonlinear form $A(\cdot,\cdot)$, we have that

$$\tilde{\alpha}\,\|(\mathbf{t}-\mathbf{t}_h,\boldsymbol{\sigma}-\boldsymbol{\sigma}_h,u-u_h)\|_X \;\le\; \sup_{\substack{(\mathbf{s},\boldsymbol{\tau},v)\in X\\(\mathbf{s},\boldsymbol{\tau},v)\neq\mathbf{0}}} \frac{R_h(\mathbf{s},\boldsymbol{\tau},v)}{\|(\mathbf{s},\boldsymbol{\tau},v)\|_X}\,, \tag{5.1}$$

where the residual R_h is defined by

$$R_h(\mathbf{s},\boldsymbol{\tau},v) := F(\mathbf{s},\boldsymbol{\tau},v) - A((\mathbf{t}_h,\boldsymbol{\sigma}_h,u_h),(\mathbf{s},\boldsymbol{\tau},v))\,, \qquad \forall\,(\mathbf{s},\boldsymbol{\tau},v)\in X\,.$$

From the definitions of F and $A(\cdot,\cdot)$, we can write

$$R_h(\mathbf{s},\boldsymbol{\tau},v) = R_1(\mathbf{s}) + R_2(\boldsymbol{\tau}) + R_3(v)\,, \tag{5.2}$$

with

$$\begin{aligned}R_1(\mathbf{s}) &:= \int_\Omega(\boldsymbol{\sigma}_h - k(\cdot,|\mathbf{t}_h|)\mathbf{t}_h)\cdot\mathbf{s} - \xi_3\int_\Omega(\nabla u_h-\mathbf{t}_h)\cdot\mathbf{s}\,,\\ R_2(\boldsymbol{\tau}) &:= \langle\boldsymbol{\tau}\cdot\mathbf{n}, g-u_h\rangle_\Gamma - \xi_2\int_\Omega(f+\nabla\cdot(\boldsymbol{\sigma}_h))\nabla\cdot\boldsymbol{\tau}\\ &\qquad + \int_\Omega(\nabla u_h-\mathbf{t}_h)\cdot\boldsymbol{\tau} - \xi_1\int_\Omega(\boldsymbol{\sigma}_h - k(\cdot,|\mathbf{t}_h|)\mathbf{t}_h)\cdot\boldsymbol{\tau}\,,\\ R_3(v) &:= \int_\Omega(f+\nabla\cdot(\boldsymbol{\sigma}_h))v - \xi_3\int_\Omega(\nabla u_h-\mathbf{t}_h)\cdot\nabla v + \xi_4\int_\Gamma(g-u_h)v\,.\end{aligned}$$

Then, using the Cauchy-Schwarz inequality, we obtain that

$$|R_1(\mathbf{s})| \le \left(\|\boldsymbol{\sigma}_h - k(\cdot,|\mathbf{t}_h|)\mathbf{t}_h\|_{[L^2(\Omega)]^2} + \xi_3\|\nabla u_h-\mathbf{t}_h\|_{[L^2(\Omega)]^2}\right)\|\mathbf{s}\|_{[L^2(\Omega)]^2}\,, \qquad \forall\,\mathbf{s}\in[L^2(\Omega)]^2\,. \tag{5.3}$$

Next, we bound $R_2(\boldsymbol{\tau})$, for $\boldsymbol{\tau}\in H(\nabla\cdot,\Omega)$. In order to deal with the term on the boundary, we consider a quasi-Helmholtz decomposition of $\boldsymbol{\tau}\in H(\nabla\cdot,\Omega)$. From [6, Lemma 5.1] we know that there exists $\chi\in H^1(\Omega)$, $\boldsymbol{\phi}\in[H^1(\Omega)]^2$, and a positive constant c such that

$$\boldsymbol{\tau} = \mathbf{curl}(\chi) + \boldsymbol{\phi}$$

ETNA
Kent State University and
Johann Radon Institute (RICAM)

and

$$\|\chi\|_{H^1(\Omega)} + \|\boldsymbol{\phi}\|_{[H^1(\Omega)]^2} \leq c\,\|\boldsymbol{\tau}\|_{H(\nabla\cdot,\Omega)}\,. \tag{5.4}$$

We remark that $\nabla\cdot\boldsymbol{\tau} = \nabla\cdot\boldsymbol{\phi}$ in Ω.

Now, let I_h be the Clément interpolation operator (cf. [10]), and let Π_h^l be the Raviart-Thomas interpolation operator (cf. [19]). Then we define $\chi_h := I_h(\chi)$ and

$$\boldsymbol{\tau}_h := \mathbf{curl}(\chi_h) + \Pi_h^l\boldsymbol{\phi}\,.$$

We remark that

$$\nabla\cdot(\boldsymbol{\tau} - \boldsymbol{\tau}_h) = (I - P_h^l)\nabla\cdot\boldsymbol{\tau}\,,$$

where $P_h^l : L^2(\Omega) \to V_h$ is the L^2-orthogonal projector. We write

$$R_2(\boldsymbol{\tau}) = R_2(\boldsymbol{\tau} - \boldsymbol{\tau}_h) = \tilde{R}_2(\boldsymbol{\tau}) + \hat{R}_2(\boldsymbol{\phi}) + \bar{R}_2(\chi)\,, \tag{5.5}$$

where

$$\begin{aligned}
\tilde{R}_2(\boldsymbol{\tau}) &= -\xi_2\int_\Omega (f + \nabla\cdot\boldsymbol{\sigma}_h)(I - P_h^l)\nabla\cdot\boldsymbol{\tau}\,,\\
\hat{R}_2(\boldsymbol{\phi}) &= \langle (I - \Pi_h^l)\boldsymbol{\phi}\cdot\mathbf{n}, g - u_h\rangle_\Gamma + \int_\Omega (\nabla u_h - \mathbf{t}_h)\cdot(I - \Pi_h^l)\boldsymbol{\phi}\\
&\qquad - \xi_1\int_\Omega (\boldsymbol{\sigma}_h - k(\cdot,|\mathbf{t}_h|)\mathbf{t}_h)\cdot(I - \Pi_h^l)\boldsymbol{\phi}\,,\\
\bar{R}_2(\chi) &= \langle \mathbf{curl}(\chi - \chi_h)\cdot\mathbf{n}, g - u_h\rangle_\Gamma + \int_\Omega (\nabla u_h - \mathbf{t}_h)\cdot\mathbf{curl}(\chi - \chi_h)\\
&\qquad - \xi_1\int_\Omega (\boldsymbol{\sigma}_h - k(\cdot,|\mathbf{t}_h|)\mathbf{t}_h)\cdot\mathbf{curl}(\chi - \chi_h)\,.
\end{aligned}$$

Next, we bound the terms in the decomposition (5.5). First, by applying the Cauchy-Schwarz inequality, we have

$$|\tilde{R}_2(\boldsymbol{\tau})| \leq \xi_2\,\|f + \nabla\cdot\boldsymbol{\sigma}_h\|_{L^2(\Omega)}\|\nabla\cdot\boldsymbol{\tau}\|_{L^2(\Omega)}\,, \tag{5.6}$$

where we used that $I - P_h^l$ is a projection. On the other hand, we can write

$$\begin{aligned}
\hat{R}_2(\boldsymbol{\phi}) = \sum_{e\in E(\Gamma)}\int_e ((I - \Pi_h^l)\boldsymbol{\phi}\cdot\mathbf{n})(g - u_h)\\
+ \sum_{T\in\mathcal{T}_h}\int_T (\nabla u_h - \mathbf{t}_h - \xi_1(\boldsymbol{\sigma}_h - k(\cdot,|\mathbf{t}_h|)\mathbf{t}_h))\cdot(I - \Pi_h^l)\boldsymbol{\phi}\,.
\end{aligned}$$

Using the Cauchy-Schwarz inequality and the approximation properties of the Raviart-Thomas interpolation operator Π_h^l, we obtain

$$\begin{aligned}
|\hat{R}_2(\boldsymbol{\phi})| &\leq c\Big(\sum_{e\in E(\Gamma)} h_e\|g - u_h\|^2_{L^2(e)} + \sum_{T\in\mathcal{T}_h} h_T^2(\|\nabla u_h - \mathbf{t}_h\|^2_{[L^2(T)]^2}\\
&\qquad + \xi_1^2\|\boldsymbol{\sigma}_h - k(\cdot,|\mathbf{t}_h|)\mathbf{t}_h\|_{[L^2(T)]^2})^2\Big)^{1/2}\|\boldsymbol{\phi}\|_{[H^1(\Omega)]^2}\\
&\leq c\Big(\sum_{e\in E(\Gamma)} h_e\|g - u_h\|^2_{L^2(e)} + \sum_{T\in\mathcal{T}_h} h_T^2(\|\nabla u_h - \mathbf{t}_h\|^2_{[L^2(T)]^2}\\
&\qquad + \xi_1^2\|\boldsymbol{\sigma}_h - k(\cdot,|\mathbf{t}_h|)\mathbf{t}_h\|_{[L^2(T)]^2})^2\Big)^{1/2}\|\boldsymbol{\tau}\|_{H(\nabla;\Omega)}\,,
\end{aligned} \tag{5.7}$$

ETNA
Kent State University and
Johann Radon Institute (RICAM)

where in the last inequality we used (5.4).

Moreover, assuming $g \in H^1(\Gamma)$,

$$|\bar{R}_2(\chi)| \le C \Big(\sum_{e\in E(\Gamma)} h_e \|\frac{d}{ds}(g-u_h)\|^2_{L^2(e)} + \sum_{T\in\mathcal{T}_h} \big(\|\nabla \mathbf{u}_h - \mathbf{t}_h\|^2_{[L^2(T)]^2} + \xi_1^2 \, \|\boldsymbol{\sigma}_h - k(\cdot,|\mathbf{t}_h|)\mathbf{t}_h\|^2_{[L^2(T)]^2} \big) \Big)^{1/2} \|\boldsymbol{\tau}\|_{H(\nabla\cdot,\Omega)} \,, \tag{5.8}$$

where $E(\Gamma)$ denotes the set of edges of the triangulation $\mathcal{T}_h$ contained in Γ, h_e denotes the length of an edge $e \in E(\Gamma)$, and $\frac{d}{ds}$ denotes the tangential derivative.

From (5.6), (5.7), and (5.8),

$$\begin{aligned} &|R_2(\boldsymbol{\tau})| \\ &\quad \le C \Big(\sum_{T\in\mathcal{T}_h} \big(\xi_2^2 \|f + \nabla\cdot\boldsymbol{\sigma}_h\|^2_{L^2(T)} + \|\nabla \mathbf{u}_h - \mathbf{t}_h\|^2_{[L^2(T)]^2} \\ &\qquad + \xi_1^2 \, \|\boldsymbol{\sigma}_h - k(\cdot,|\mathbf{t}_h|)\mathbf{t}_h\|^2_{[L^2(T)]^2} \big) \\ &\qquad + \sum_{e\in E(\Gamma)} h_e \big(\|g-u_h\|^2_{L^2(e)} + \|\frac{d}{ds}(g-u_h)\|^2_{L^2(e)} \big) \Big)^{1/2} \|\boldsymbol{\tau}\|_{H(\nabla\cdot,\Omega)} \,. \end{aligned} \tag{5.9}$$

Finally, using the orthogonality property and the approximation properties of the Clément interpolation operator (see, for instance, [4]) yields

$$\begin{aligned} |R_3(v)| \le C \Big(&\sum_{T\in\mathcal{T}_h} \big(h_T^2 \|f + \nabla\cdot\boldsymbol{\sigma}_h\|^2_{L^2(T)} + \xi_3^2 \|\nabla u_h - \mathbf{t}_h\|^2_{[L^2(T)]^2} \big) \\ &+ \xi_4^2 \sum_{e\in E(\Gamma)} h_e \|g-u_h\|^2_{L^2(e)} \Big)^{1/2} \|v\|_{H^1(\Omega)}. \end{aligned} \tag{5.10}$$

Then we define on any triangle $T \in \mathcal{T}_h$ the following a posteriori error indicator:

$$\begin{aligned} \theta_T^2 := \|\nabla u_h - \mathbf{t}_h\|^2_{[L^2(T)]^2} + \|f + \nabla\cdot\boldsymbol{\sigma}_h\|^2_{L^2(T)} + \|\boldsymbol{\sigma}_h - k(\cdot,|\mathbf{t}_h|)\mathbf{t}_h\|^2_{[L^2(T)]^2} \\ + \sum_{e\in E(T)\cap E(\Gamma)} h_e \big(\|g-u_h\|^2_{L^2(e)} + \|\frac{d}{ds}(g-u_h)\|^2_{L^2(e)} \big) \,, \end{aligned} \tag{5.11}$$

where $E(T)$ denotes the set of edges of T. We also define the global a posteriori error indicator θ with

$$\theta^2 := \sum_{T\in\mathcal{T}_h} \theta_T^2.$$

From the previous results, we have the following theorem.

THEOREM 5.1. *Assume $g \in H^1(\Gamma)$. Then there exists a positive constant $C_{\mathtt{rel}}$, independent of h, such that*

$$\|(\mathbf{t}-\mathbf{t}_h, \boldsymbol{\sigma}-\boldsymbol{\sigma}_h, u-u_h)\|_X \le C_{\mathtt{rel}} \, \theta \,.$$

Proof. The result follows from inequality (5.1), the decomposition (5.2), the triangle inequality, and the bounds (5.3), (5.9), and (5.10) together with the definition of θ with $C_{\mathtt{rel}} := C \, \tilde{\alpha}^{-1} \, \max(1, \xi_1, \xi_2, \xi_3, \xi_4)$ (C is independent of h and the stabilisation parameters). ∎

ETNA
Kent State University and
Johann Radon Institute (RICAM)

Let us now prove the local efficiency of the a posteriori error indicator θ_T. Given $e \in E(\Gamma)$, we denote by ψ_e the usual edge-bubble function and by $L : \mathcal{C}(e) \to \mathcal{C}(T_e)$ the extension operator as defined in [20]. We also recall the following lemma from [20].

LEMMA 5.2. *Given $m \in \mathbb{N} \cup \{0\}$, there exist positive constants C_2 and C_3 depending only on m and the shape regularity of the triangulations such that for each $T \in \mathcal{T}_h$ and $e \in E(T)$,*

$$\|p\|^2_{L^2(e)} \leq C_2 \, \|\psi_e^{1/2} p\|^2_{L^2(e)} \,, \qquad \forall\, p \in \mathcal{P}_m(e) \,, \tag{5.12}$$

$$\|\psi_e^{1/2} L(p)\|^2_{L^2(T)} \leq C_3 \, h_e \, \|p\|^2_{L^2(e)} \,, \qquad \forall\, p \in \mathcal{P}_m(e) \,. \tag{5.13}$$

Proof. See [20, Lemma 4.1]. ∎

THEOREM 5.3. *Assume that g is piecewise polynomial on Γ. Then there exists a positive constant $C_{\mathtt{eff}}$, independent of h and T, such that for all $T \in \mathcal{T}_h$,*

$$C_{\mathtt{eff}} \, \theta_T \leq \|(\mathbf{t} - \mathbf{t}_h, \boldsymbol{\sigma} - \boldsymbol{\sigma}_h, u - u_h)\|_{[L^2(T)]^2 \times H(\nabla\cdot, T) \times H^1(T)} \,.$$

Proof. Let $T \in \mathcal{T}_h$. We first use that $\mathbf{t} = \nabla u$, $f = -\nabla \cdot \boldsymbol{\sigma}$, and $\boldsymbol{\sigma} = k(\cdot, |\mathbf{t}|)\mathbf{t}$ in Ω and the triangle inequality to obtain

$$\begin{aligned} \|\nabla u_h - \mathbf{t}_h\|^2_{[L^2(T)]^2} &\leq 2\|\nabla(u_h - u)\|^2_{[L^2(T)]^2} + 2\|\mathbf{t} - \mathbf{t}_h\|^2_{[L^2(T)]^2}, \\ \|f + \nabla \cdot \boldsymbol{\sigma}_h\|^2_{L^2(T)} &= \|\nabla \cdot (\boldsymbol{\sigma}_h - \boldsymbol{\sigma})\|^2_{L^2(T)}, \\ \|\boldsymbol{\sigma}_h - k(\cdot, |\mathbf{t}_h|)\mathbf{t}_h\|^2_{[L^2(T)]^2} &\leq 2\|\boldsymbol{\sigma}_h - \boldsymbol{\sigma}\|^2_{[L^2(T)]^2} + 8\, k_2^2 \, \|\mathbf{t} - \mathbf{t}_h\|^2_{[L^2(T)]^2}, \end{aligned} \tag{5.14}$$

where in the last inequality we used (3.5).

In order to bound the first boundary term, we proceed as in [3, Lemma 3.7] and use the following discrete trace inequality (see [1, Theorem 3.10]):

$$\|v\|^2_{L^2(e)} \leq C_t \, (h_e^{-1} \|v\|^2_{L^2(T)} + h_e |v|^2_{H^1(T)}) \,, \qquad \forall\, v \in H^1(T) \,,$$

where T is any triangle such that $e \in E(T)$. Then we obtain

$$h_e \, \|g - u_h\|^2_{L^2(e)} \leq C_t \left(\|u - u_h\|^2_{L^2(T_e)} + h^2_{T_e} \, |u - u_h|^2_{H^1(T_e)} \right), \tag{5.15}$$

where T_e is the triangle having e as an edge.

Finally, to bound the second term on the boundary, we proceed as in [3, Lemma 3.9]. Let $\chi_e := \frac{d}{ds}(g - u_h)$ on e. Then, using (5.12), the extension operator L, and integrating by parts, we have that

$$\begin{aligned} ||\chi_e||^2_{L^2(e)} \leq C_2 \, ||\psi_e^{1/2} \chi_e||^2_{L^2(e)} &= C_2 \int_{\partial T_e} \psi_e \, L(\chi_e) \nabla(u - u_h) \cdot \mathbf{T} \\ &= C_2 \int_{T_e} \mathbf{curl}(\psi_e L(\chi_e)) \cdot \nabla(u - u_h) \,, \end{aligned}$$

where $\mathbf{T}$ denotes the tangent vector. Applying the Cauchy-Schwarz inequality, an inverse inequality, and inequality (5.13), we obtain

$$\begin{aligned} ||\chi_e||^2_{L^2(e)} &\leq C_2 \, |\psi_e L(\chi_e)|_{H^1(T_e)} \, |u - u_h|_{H^1(T_e)} \\ &\leq C_2 C \, h_e^{-1} ||\psi_e L(\chi_e)||_{L^2(T_e)} \, |u - u_h|_{H^1(T_e)} \\ &\leq C_4 \, h_e^{-1/2} ||\chi_e||_{L^2(e)} \, |u - u_h|_{H^1(T_e)} \,, \end{aligned}$$

ETNA
Kent State University and
Johann Radon Institute (RICAM)

where $C_4 := C_2CC_3$ depends only on m and the shape regularity of the triangulations. Therefore,

$$h_e \, \| \frac{d}{ds}(g - u_h) \|^2_{L^2(e)} \leq C_4 \, |u - u_h|^2_{H^1(T_e)} \, , \tag{5.16}$$

and the local efficiency follows from inequalities (5.14), (5.15), and (5.16) with $C_{\mathtt{eff}} = \max(2 + 8k_2^2, C_t + C_4)$. ∎

6. Numerical experiments. In this section, we provide some numerical experiments that confirm the theoretical results from the previous sections. We have implemented an adaptive algorithm based on the a posteriori error indicator θ_T defined in (5.11) in a FreeFem++ code [13] and tested it for several examples. The adaptive algorithm reads as follows:

1. Start with a coarse mesh $\mathcal{T}_h$.
2. Solve the Galerkin scheme (4.1) for the current mesh $\mathcal{T}_h$.
3. Compute θ_T for each triangle $T \in \mathcal{T}_h$.
4. Consider a stopping criterion and decide to finish or go to the next step.
5. Use the `adaptmesh` FreeFem++ function to build a new mesh $\mathcal{T}_h$ and go to step 2.

We start the adaptive algorithm with a coarse mesh. Then, in every adaptive step, we rebuild the mesh and control its shape-regularity by bounding the gradient of the mesh size function; for more details, see [5]. The Galerkin scheme (4.1) is a nonlinear algebraic system, which is solved by means of Newton's method. We consider the finite element spaces S_h, H_h, and V_h defined in (4.3)–(4.5) for $m = 0$ and $l = 0$, so that for a smooth solution the expected rate of convergence is 1.

In what follows, $\mathcal{N}$ stands for the total number of degrees of freedom (DOF) of the Galerkin scheme (4.1). We consider the individual errors

$$e(u) := \|u - u_h\|_{H^1(\Omega)} \, , \qquad e(\mathbf{t}) := \|\mathbf{t} - \mathbf{t}_h\|_{[L^2(\Omega)]^2} \, , \qquad e(\boldsymbol{\sigma}) := \|\boldsymbol{\sigma} - \boldsymbol{\sigma}_h\|_{H(\nabla\cdot,\Omega)}$$

and define the total error

$$e_{\mathtt{total}} := \left(e(u)^2 + e(\mathbf{t})^2 + e(\boldsymbol{\sigma})^2 \right)^{1/2}.$$

We denote by $r_{\mathtt{total}}$ the experimental rate of convergence; for the uniform refinement, $r_{\mathtt{total}}$ is defined by

$$r_{\mathtt{total}} := \frac{\log(e_{\mathtt{total}}/e'_{\mathtt{total}})}{\log(h/h')} \, ,$$

where $e_{\mathtt{total}}$ and $e'_{\mathtt{total}}$ are the total errors for two consecutive triangulations with mesh sizes h and h', respectively. For the adaptive refinement,

$$r_{\mathtt{total}} := -2 \, \frac{\log(e_{\mathtt{total}}/e'_{\mathtt{total}})}{\log(\mathcal{N}/\mathcal{N}')} \, ,$$

where $\mathcal{N}$ and $\mathcal{N}'$ denote the corresponding DOF of each triangulation. Finally, we denote by I_θ the effectivity index with respect to θ, $I_\theta := e_{\mathtt{total}}/\theta$.

We consider four examples. First, we test the robustness of the adaptive algorithm with respect to the stabilisation parameters ξ_1, ξ_2, ξ_3, and ξ_4. Then we consider two academic examples with a known solution. In Example 2, the solution has a singularity close to a boundary point. In Example 3, the solution has a singularity close to a line. Finally, in Example 4, we apply the adaptive algorithm to solve a magnetostatic problem. In all cases, we

ETNA
Kent State University and
Johann Radon Institute (RICAM)

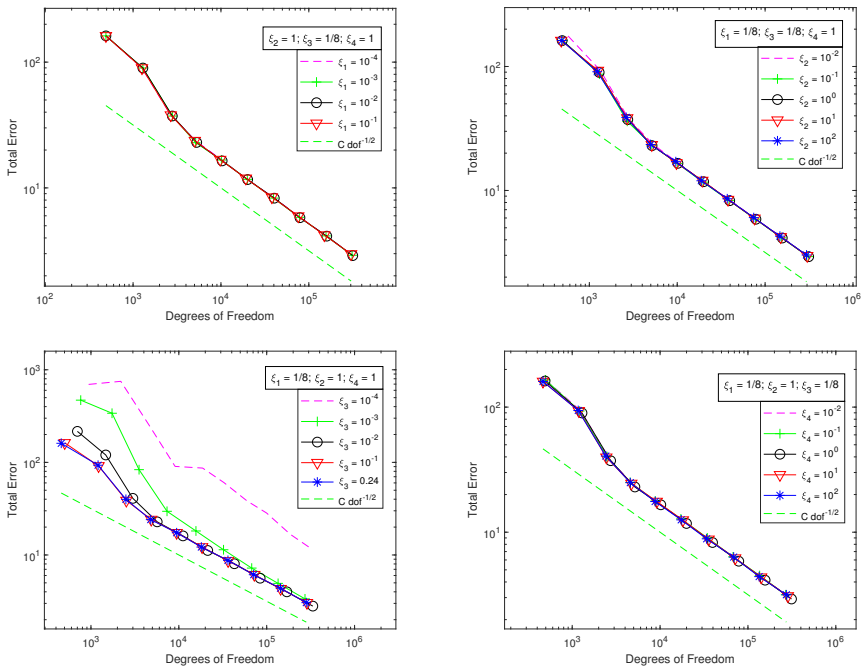

FIG. 6.1. *Example 1: Sensitivity of the adaptive method with respect to the stabilisation parameters.*

choose as initial guess in the Newton's method the solution of the corresponding linearized problem; Newton's method requires 4 iterations to attain a relative tolerance of 10^{-9}.

EXAMPLE 1. In order to test the sensitivity of the error indicator with respect to the stabilisation parameters, we consider $\Omega = (-1,1)^2 \setminus [0,1]^2$ and take $k(\mathbf{x},s) = \frac{s+1}{s+2}$. We choose f and g so that the exact solution is $u(x,y) = (x-1.1)^{-1}$, $(x,y) \in \Omega$. In this case, the values of the stabilisation parameters that ensure strong monotonicity of the nonlinear form are $\xi_1 \in (0, \frac{1}{4})$, $\xi_2 > 0$, $\xi_3 \in (0, \frac{1}{4})$, and $\xi_4 > 0$. We made four experiments. In each experiment, we fixed the value of three stabilisation parameters and vary the remaining one. The results are presented in Figure 6.1. As can be seen from these graphs, in all cases optimal rates of convergence are attained independently of the values of the stabilisation parameters. However, we remark that convergence is affected as the stabilisation parameter ξ_3 gets smaller and smaller.

EXAMPLE 2. We let $\Omega = (0,1) \times (0,1)$ be the unit square and choose f and g so that the exact solution is $u(x,y) = (2.1 - x - y)^{-1/3}$. We remark that the solution u has a singularity close to the boundary point $(1,1)$. We take $k(\mathbf{x},s) = 2 + \frac{1}{s+1}$ and choose $\xi_1 = 1/18$, $\xi_2 = 1$, $\xi_3 = 1/2$, and $\xi_4 = 1$. In Tables 6.1 and 6.2 we provide the DOF, the individual and total errors, the experimental rates of convergence, the a posteriori error indicators, and the effectivity indices for the uniform and adaptive refinements, respectively. We appreciate that the adaptive refinement algorithm shows better convergence properties than the uniform refinement algorithm (see also Figure 6.2). Moreover, the efficiency indices are very close to 1. In Figure 6.3 we depict the different terms that make up the indicator θ with respect to the

ETNA
Kent State University and
Johann Radon Institute (RICAM)

TABLE 6.1
Example 2, uniform refinement: Individual and total errors, experimental rates of convergence, a posteriori error indicators and effectivity indices.

$\mathcal{N}$	$\mathcal{N}^{-1/2}$	$e(u)$	$e(\mathbf{t})$	$e(\boldsymbol{\sigma})$	$e_{\texttt{total}}$	$r_{\texttt{total}}$	θ	I_θ
195	7.161E-02	3.992E-01	2.694E-01	7.154E+00	7.171E+00	—	8.111E+00	1.1312
579	4.156E-02	2.131E-01	1.350E-01	5.369E+00	5.375E+00	0.416	5.523E+00	1.0275
2069	2.198E-02	1.068E-01	6.591E-02	3.239E+00	3.241E+00	0.730	3.270E+00	1.0090
7357	1.166E-02	5.386E-02	3.427E-02	1.730E+00	1.732E+00	0.885	1.746E+00	1.0081
30069	5.767E-03	2.712E-02	1.798E-02	8.819E-01	8.825E-01	0.994	8.776E-01	0.9945
117659	2.915E-03	1.357E-02	9.247E-03	4.432E-01	4.435E-01	0.993	4.409E-01	0.9942
458119	1.477E-03	6.777E-03	4.681E-03	2.219E-01	2.220E-01	0.977	2.226E-01	1.0028

TABLE 6.2
Example 2, adaptive refinement: Individual and total errors, experimental rates of convergence, a posteriori error indicators and effectivity indices.

$\mathcal{N}$	$\mathcal{N}^{-1/2}$	$e(u)$	$e(\mathbf{t})$	$e(\boldsymbol{\sigma})$	$e_{\texttt{total}}$	$r_{\texttt{total}}$	θ	I_θ
195	7.161E-02	3.992E-01	2.694E-01	7.154E+00	7.171E+00	—	8.111E+00	1.1312
397	5.019E-02	9.480E-02	9.703E-02	3.078E+00	3.081E+00	2.377	3.099E+00	1.0059
757	3.635E-02	5.294E-02	7.065E-02	1.358E+00	1.361E+00	2.533	1.366E+00	1.0039
1379	2.693E-02	3.931E-02	5.488E-02	8.673E-01	8.699E-01	1.492	8.821E-01	1.0140
2705	1.923E-02	2.838E-02	4.021E-02	6.229E-01	6.249E-01	0.982	6.349E-01	1.0160
5389	1.362E-02	2.105E-02	2.861E-02	4.482E-01	4.496E-01	0.955	4.549E-01	1.0116
10595	9.715E-03	1.438E-02	2.029E-02	3.173E-01	3.182E-01	1.023	3.211E-01	1.0088
21391	6.837E-03	1.030E-02	1.446E-02	2.241E-01	2.248E-01	0.989	2.275E-01	1.0121
41407	4.914E-03	7.007E-03	1.006E-02	1.563E-01	1.567E-01	1.092	1.586E-01	1.0119
84861	3.433E-03	5.075E-03	7.277E-03	1.122E-01	1.125E-01	0.923	1.138E-01	1.0115
165147	2.461E-03	3.557E-03	5.029E-03	7.812E-02	7.836E-02	1.087	7.917E-02	1.0103
338177	1.720E-03	2.529E-03	3.604E-03	5.587E-02	5.604E-02	0.936	5.664E-02	1.0106
656523	1.234E-03	1.755E-03	2.511E-03	3.884E-02	3.896E-02	1.096	3.935E-02	1.0100

DOF. We denote

$$\theta_1^2 := \sum_{T\in\mathcal{T}_h} \|\nabla u_h - \mathbf{t}_h\|^2_{[L^2(T)]^2}\,,$$
$$\theta_2^2 := \sum_{T\in\mathcal{T}_h} \|f + \nabla\cdot\boldsymbol{\sigma}_h\|^2_{L^2(T)}\,,$$
$$\theta_3^2 := \sum_{T\in\mathcal{T}_h} \|\boldsymbol{\sigma}_h - k(\cdot,|\mathbf{t}_h|)\mathbf{t}_h\|^2_{[L^2(T)]^2}\,,$$
$$\theta_4^2 := \sum_{e\in E(\Gamma)} h_e\left(\|g-u_h\|^2_{L^2(e)} + \|\frac{d}{ds}(g-u_h)\|^2_{L^2(e)}\right)\,.$$

We observe that the second term, which represents the residual in the equilibrium equation, is the dominating one. Finally, in Figure 6.4, we plot the initial mesh and some adapted meshes. We observe that the meshes are highly refined around the corner $(1,1)$.

EXAMPLE 3. We let $\Omega = (-1,1)\times(-1,1)$ and choose f and g so that the exact solution is $u(x,y) = (x-1.1)^{-1}$. In this case, the solution u has a singularity around the line $x=1$. We take $k(\mathbf{x},s) = 2 + \frac{1}{s+1}$ and choose $\xi_1 = 1/18$, $\xi_2 = 1$, $\xi_3 = 1/2$, and $\xi_4 = 1$. In Tables 6.3 and 6.4 we present the DOF, the individual and total errors, the experimental rates of convergence, the a posteriori error indicators, and the effectivity indices for the uniform and adaptive refinements, respectively. As in the previous example, the adaptive refinement algorithm shows better convergence properties than the uniform refinement algorithm (see also Figure 6.5), and the efficiency indices are again very close to 1. In this case, as can be seen from Figure 6.6, the residual in the equilibrium equation is again the dominating term

ETNA
Kent State University and
Johann Radon Institute (RICAM)

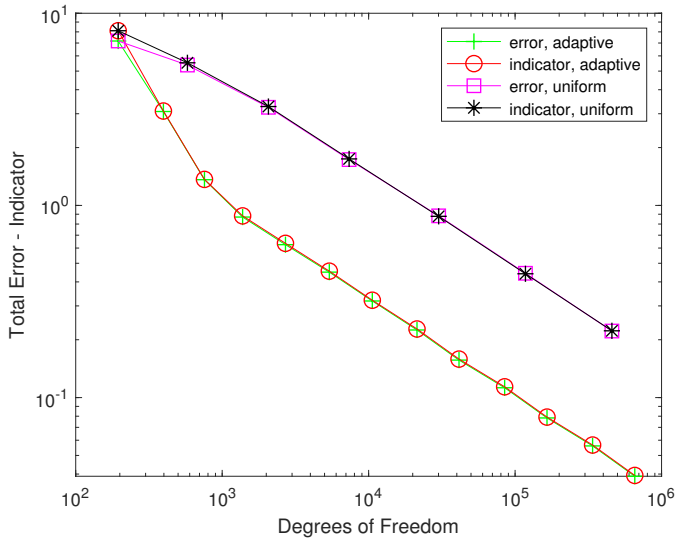

FIG. 6.2. *Example 2: Error and indicator vs. DOFs for uniform and adaptive refinements.*

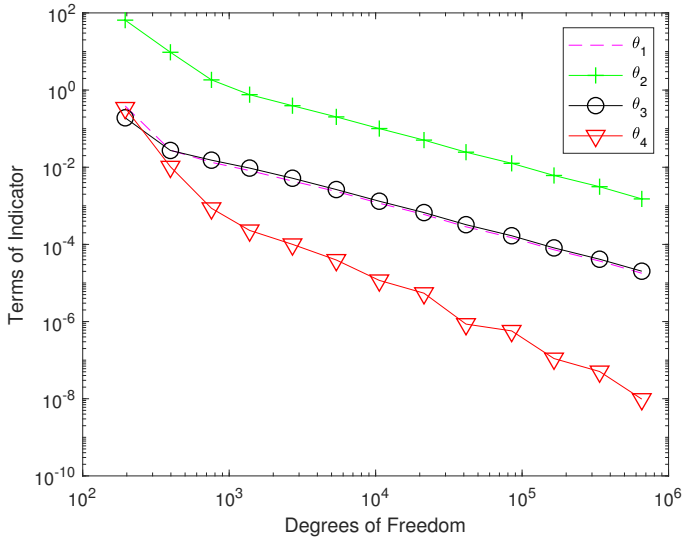

FIG. 6.3. *Example 2: Terms of the indicator vs. DOFs for adaptive refinement.*

in θ. In Figure 6.7, we display the initial mesh and some adapted meshes. In this case, the adaptive algorithm refines the meshes around the line $x = 1$, that is, close to the singularity of the solution.

EXAMPLE 4. Inspired by [14], we tested the method proposed in this paper on an example regarding a direct current motor. Let $\Omega = \bigcup_j \Omega_j$ represent the cross-section of a motor (see Figure 6.8), with Ω_j being materials with different magnetic properties.

Direct current motors have inside a permanent magnet. In Figure 6.8 the permanent magnet corresponds to the two pieces named N and S, which stand for north pole and south pole, respectively. The motor is mounted inside an outer housing (O.H.) of ferromagnetic

ETNA
Kent State University and
Johann Radon Institute (RICAM)

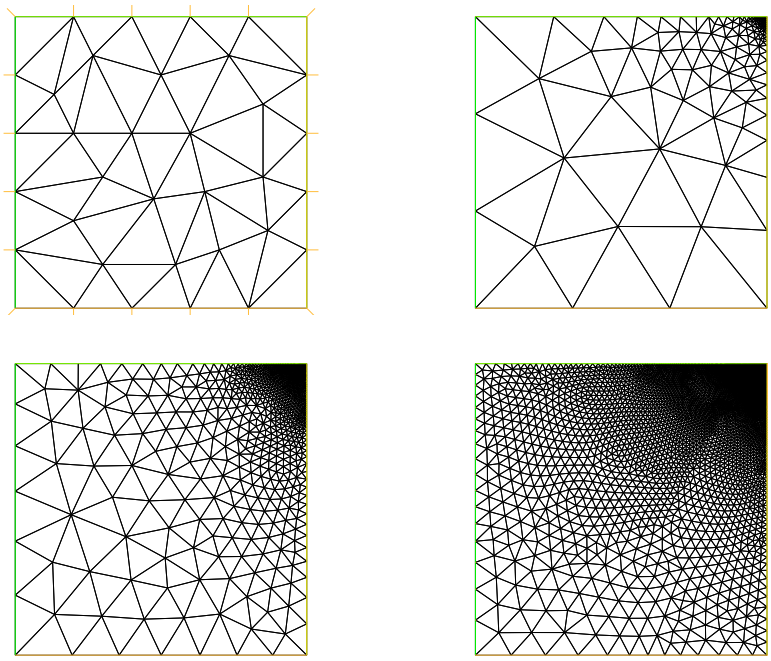

FIG. 6.4. *Example 2 (from top left to bottom right): Initial mesh (*195 *DOF) and intermediate adapted meshes with* 1379, 10595, *and* 84861 *DOF, respectively.*

material. The core element is the rotor, a star-shaped piece with twelve branches, also made of ferromagnetic material. Between every two adjacent branches there is a winding, denoted as J_i, $i = 1, \ldots, 12$. The rest of the domain is composed of air. The central circle represents the axis of rotation and is not included in the domain.

We solve the boundary value problem (2.1) with $f = S + \frac{\partial H_y}{\partial x} - \frac{\partial H_x}{\partial y}$ in each subdomain Ω_j, where S represents the z-component of the current density, $\mathbf{H} = (H_x, H_y, 0)^\mathsf{t}$ represents the magnetization of the permanent magnets, and u is the z-component of the vector potential $\mathbf{A}$. The function $k(\mathbf{x}, s)$ represents the inverse of the magnetic permeability; we take $k(\mathbf{x}, s) := 200 + \frac{5000}{1+0.05\, s^2}$ in the ferromagnetic material and $k(\mathbf{x}, s) := 8 \times 10^5\, m/H$ elsewhere. We apply homogeneous Dirichlet boundary conditions ($g = 0$) and take the same parameters as in [14]: the outer housing has an external diameter of $50\, mm$. The windings J_1 and J_7 have no current density ($S = 0$), J_2, J_3, J_4, J_5, and J_6 have a current density $S = -375\, Acm^{-2}$, and for J_8, J_9, J_{10}, J_{11}, and J_{12}, the current density is $S = 375\, Acm^{-2}$. The magnets have a radial permanent magnetic field of $0.4\, T$.

In this case, we take the following values for the stabilisation parameters: $\xi_1 = 1/4$, $\xi_2 = 1$, $\xi_3 = 1/4$, and $\xi_4 = 0$. For the adaptive meshing routine, we started from an initial mesh of 27 328 degrees of freedom. The algorithm generates a new mesh with 236 614 degrees of freedom after 4 iterations. The initial and final meshes can be seen in Figure 6.9. For each individual mesh, the corresponding nonlinear problem is solved by means of Newton's method with a stopping criterion based on the relative error with a tolerance of 10^{-9}. Newton's method converged after 5 iterations.

The magnetic equipotential lines are represented in Figure 6.10. They consist of closed lines that go from the core's central circle to the outer housing, passing through the branches and both permanent magnets, following radial directions. The main goal of the outer housing is exactly to allow for the magnetic lines to close therein. The magnetic line density is higher

ETNA
Kent State University and
Johann Radon Institute (RICAM)

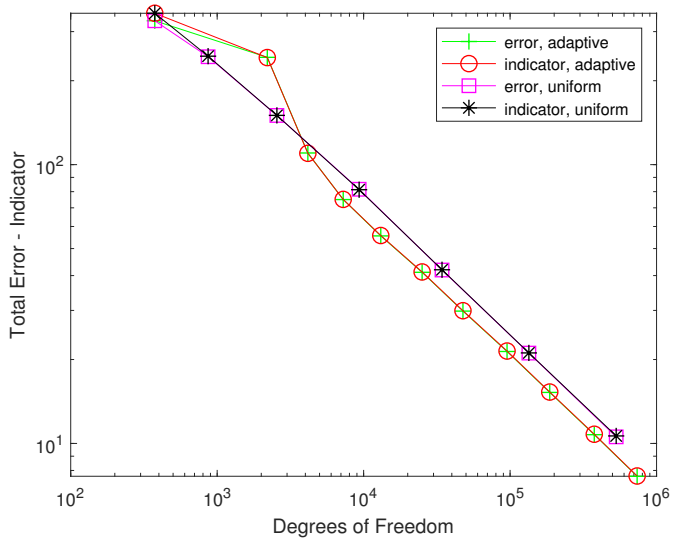

FIG. 6.5. *Example 3: Error and indicator vs. DOFs for uniform and adaptive refinements.*

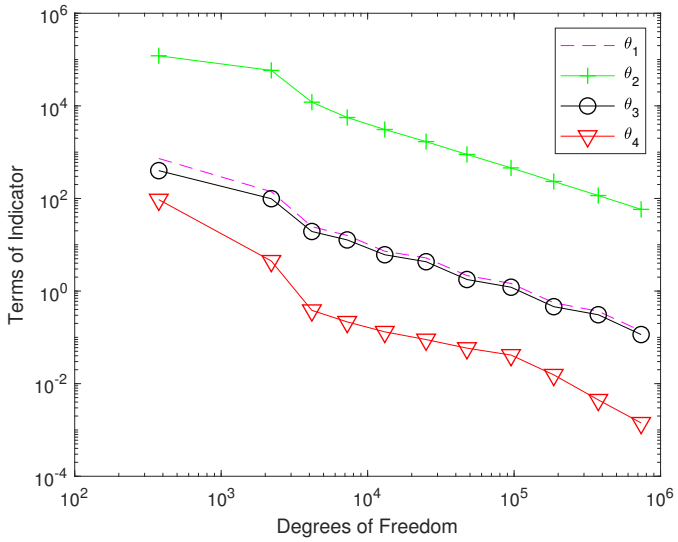

FIG. 6.6. *Example 3: Terms of the indicator vs. DOFs for adaptive refinement.*

in those branches closer to the permanent magnets, and in some areas of the outer housing where they are forced to pass through. This higher density represents a higher error, which is detected by the error indicator, and the mesh density is adjusted accordingly, as can be seen in comparison with Figure 6.10. Finally, Figure 6.11 displays the values of the error indicator versus the degrees of freedoms comparing adaptive and uniform refinement.

ETNA
Kent State University and
Johann Radon Institute (RICAM)

TABLE 6.3
Example 3, uniform refinement: Individual and total errors, experimental rates of convergence, a posteriori error indicators and effectivity indices.

$\mathcal{N}$	$\mathcal{N}^{-1/2}$	$e(u)$	$e(\mathbf{t})$	$e(\boldsymbol{\sigma})$	$e_{\texttt{total}}$	$r_{\texttt{total}}$	θ	I_θ
375	5.164E-02	1.554E+01	1.635E+01	3.272E+02	3.281E+02	—	3.491E+02	1.0641
867	3.396E-02	7.026E+00	9.565E+00	2.435E+02	2.438E+02	0.429	2.449E+02	1.0047
2557	1.978E-02	2.961E+00	4.937E+00	1.500E+02	1.501E+02	0.700	1.502E+02	1.0004
9317	1.036E-02	1.305E+00	2.484E+00	8.155E+01	8.160E+01	0.879	8.130E+01	0.9963
34293	5.400E-03	6.136E-01	1.247E+00	4.186E+01	4.188E+01	0.962	4.197E+01	1.0022
134347	2.728E-03	2.991E-01	6.252E-01	2.108E+01	2.109E+01	0.990	2.112E+01	1.0015
530109	1.373E-03	1.481E-01	3.129E-01	1.056E+01	1.056E+01	0.997	1.064E+01	1.0068

TABLE 6.4
Example 3, adaptive refinement: Individual and total errors, experimental rates of convergence, a posteriori error indicators and effectivity indices.

$\mathcal{N}$	$\mathcal{N}^{-1/2}$	$e(u)$	$e(\mathbf{t})$	$e(\boldsymbol{\sigma})$	$e_{\texttt{total}}$	$r_{\texttt{total}}$	θ	I_θ
375	5.164E-02	1.554E+01	1.635E+01	3.272E+02	3.281E+02	—	3.491E+02	1.0641
2199	2.132E-02	4.923E+00	7.785E+00	2.425E+02	2.426E+02	0.341	2.421E+02	0.9980
4161	1.550E-02	2.132E+00	3.118E+00	1.101E+02	1.101E+02	2.477	1.098E+02	0.9969
7253	1.174E-02	1.679E+00	2.530E+00	7.488E+01	7.494E+01	1.386	7.505E+01	1.0014
13093	8.739E-03	1.126E+00	1.716E+00	5.547E+01	5.551E+01	1.017	5.569E+01	1.0033
25077	6.315E-03	9.695E-01	1.425E+00	4.106E+01	4.110E+01	0.925	4.122E+01	1.0031
47657	4.581E-03	6.179E-01	9.129E-01	2.981E+01	2.983E+01	0.998	2.993E+01	1.0034
95323	3.239E-03	5.070E-01	7.459E-01	2.135E+01	2.137E+01	0.962	2.145E+01	1.0036
186505	2.316E-03	3.079E-01	4.594E-01	1.523E+01	1.524E+01	1.008	1.529E+01	1.0035
375619	1.632E-03	2.443E-01	3.738E-01	1.074E+01	1.075E+01	0.996	1.079E+01	1.0034
736783	1.165E-03	1.480E-01	2.290E-01	7.621E+00	7.626E+00	1.020	7.643E+00	1.0022

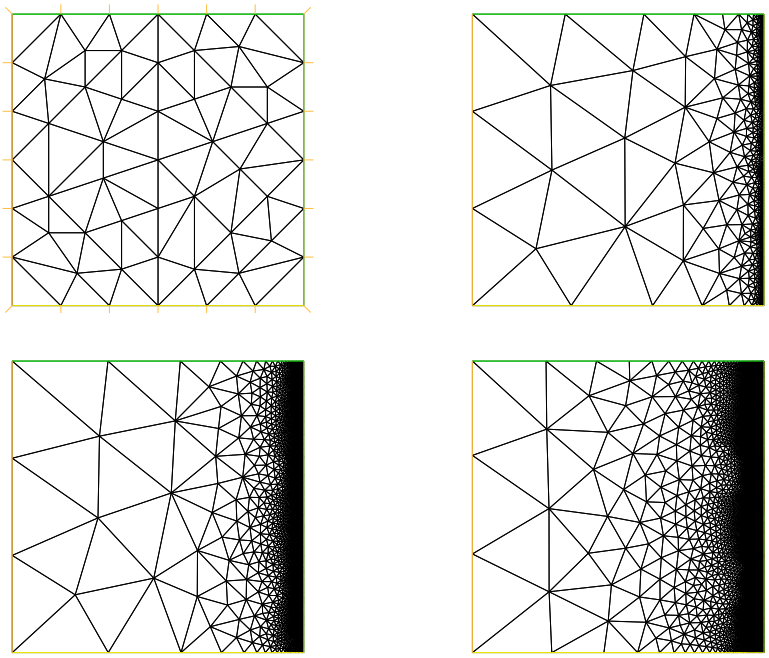

FIG. 6.7. *Example 3 (from top left to bottom right): Initial mesh (*375 *DOF) and intermediate adapted meshes with* 4161, 25077, *and* 95323 *DOF.*

ETNA
Kent State University and
Johann Radon Institute (RICAM)

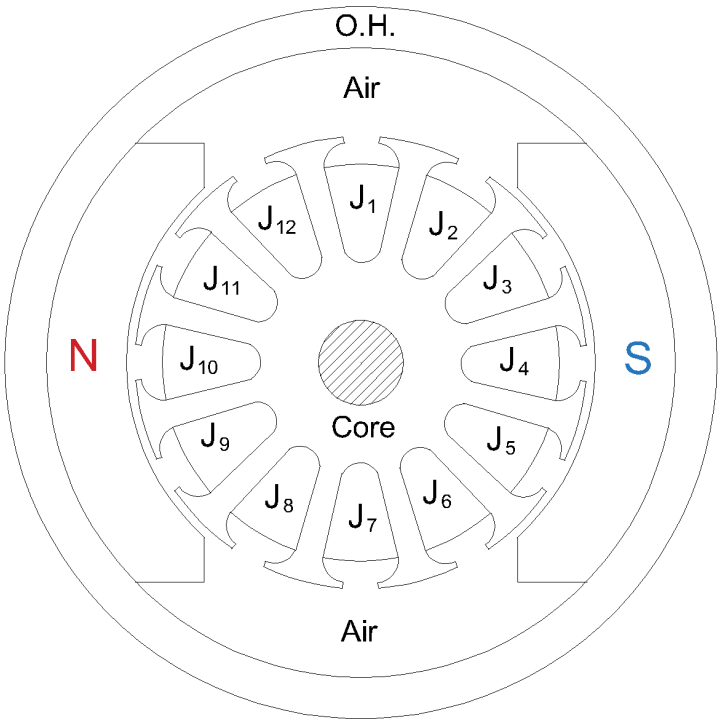

FIG. 6.8. *Example 4: Cross section of the simulated direct current motor. O.H.: outer housing, J_i: wirings, N: permanent magnet north pole, S: permanent magnet south pole.*

7. Conclusions. We propose a new adaptive stabilised Galerkin scheme to solve a nonlinear problem with a Lipschitz continuous and strongly monotone operator. We show that the discrete augmented methods is well-posed and that a Céa-type estimate holds. We also derive a rate of convergence result when globally continuous piecewise polynomials are used to approximate the primary unknown, piecewise polynomials are used to approximate its gradient, and Raviart-Thomas elements are used to approximate the nonlinear flux. We develop an a posteriori error analysis of residual type and obtain an a posteriori error indicator which is reliable and locally efficient. Finally, we provide some numerical experiments that support the theoretical results, including the application of the adaptive algorithm to the computation of the magnetic field in a direct current motor.

Acknowledgements. The authors acknowledge the support of CITIC, a Research Center of the Galician university system financed by Consellería de Educación, Universidade e Formación Profesional da Xunta de Galicia through Fondo Europeo de Desenvolvemento Rexional (FEDER) at 80%, operative program FEDER Galicia 2014-2020 and at the remaining 20% from Secretaría Xeral de Universidades (grant ED431G 2019/01). Moreover, the research of M.G. was partially supported by Xunta de Galicia Grant GRC ED431C 2018-033. The research of H.V. was partially supported by Xunta de Galicia Grant ED481A-2019/413170 and Ministerio de Educación Grant FPU18/06125.

ETNA
Kent State University and
Johann Radon Institute (RICAM)

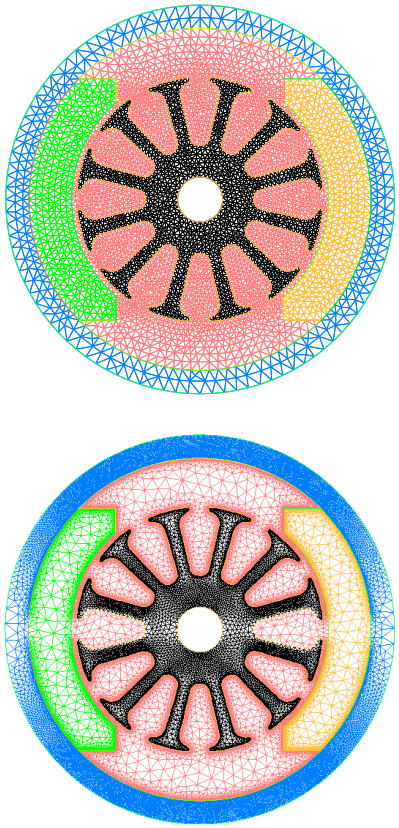

FIG. 6.9. *Example 4: Initial mesh with* 27 328 *DOF and final adapted mesh after* 4 *iterations with* 236 614 *DOF.*

REFERENCES

[1] S. AGMON, *Lectures on Elliptic Boundary Value Problems*, Van Nostrand, Princeton, 1965.
[2] R. ARAYA, T. P. BARRIOS, G. N. GATICA, AND N. HEUER, *A posteriori error estimates for a mixed-FEM formulation of a non-linear elliptic problem*, Comput. Methods Appl. Mech. Eng., 191 (2002), pp. 2317–2336.
[3] T. P. BARRIOS, R. BUSTINZA, G. C. GARCÍA, AND M. GONZÁLEZ, *A posteriori error analyses of a velocity-pseudostress formulation of the generalized Stokes problem*, J. Comput. Appl. Math., 357 (2019), pp. 349–365.
[4] T. P. BARRIOS, J. M. CASCÓN, AND M. GONZÁLEZ, *On an adaptive stabilized mixed finite element method for the Oseen problem with mixed boundary conditions*, Comput. Methods Appl. Mech. Engrg., 365 (2020), Art. 113007, 21 pages.
[5] H. BOROUCHAKI, F. HECHT, AND P. J. FREY, *Mesh gradation control*, Internat. J. Numer. Methods Engrg., 43 (1998), pp. 1143–1165.
[6] J. M. CASCÓN, R. H. NOCHETTO, AND K. G. SIEBERT, *Design and Convergence of AFEM in $H(div)$*, Math. Models Methods Appl. Sci., 17 (2007), pp. 1849–1881.
[7] Z. CHEN, *Expanded mixed finite element methods for linear second-order elliptic problems. I*, RAIRO Modél. Math. Anal. Numér., 32 (1998), pp. 479–499.
[8] ———*Expanded mixed finite element methods for quasilinear second-order elliptic problems. II*, RAIRO Modél. Math. Anal. Numér., 32 (1998), pp. 501–520.
[9] P. G. CIARLET, *The Finite Element Method for Elliptic Problems*, SIAM, Philadelphia, 2002.
[10] P. CLÉMENT, *Approximation by finite element functions using local regularisation*, Rev. Française Automat. Informat. Recherche Opérationnelle Sér., 9 (1975), pp. 77–84.

ETNA
Kent State University and
Johann Radon Institute (RICAM)

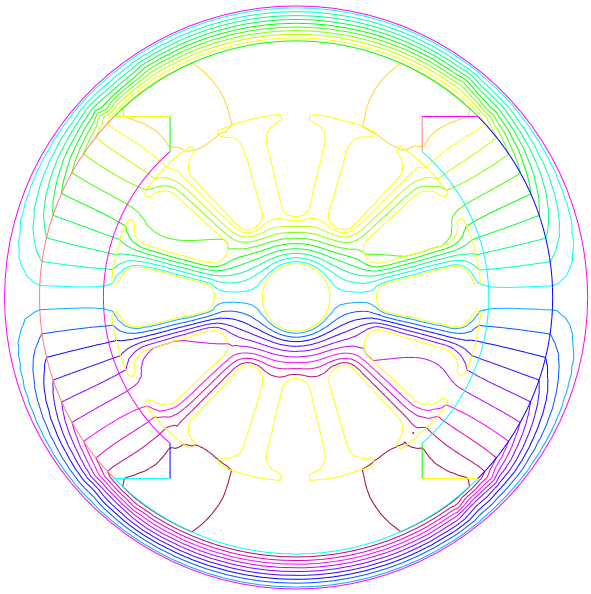

FIG. 6.10. *Example 4: Magnetic potential lines obtained with the final mesh.*

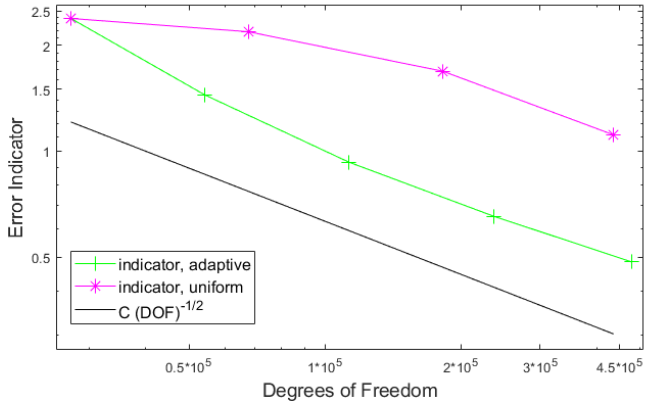

FIG. 6.11. *Example 4: Error indicator vs. DOFs for uniform and adaptive refinements.*

[11] A. I. GARRALDA-GUILLEM, M. RUIZ GALÁN, G. N. GATICA, AND A. MÁRQUEZ, *A posteriori error analysis of twofold saddle point variational formulations for nonlinear boundary value problems*, IMA J. Numer. Anal., 34 (2014), pp. 326–361.
[12] G. N. GATICA, N. HEUER, AND S. MEDDAHI, *On the numerical analysis of nonlinear twofold saddle point problems*, IMA J. Numer. Anal., 23 (2003), pp. 301–330.
[13] F. HECHT, *New development in freefem++*, J. Numer. Math., 20 (2012), pp. 251–265.
[14] B. HEISE, *Nonlinear field calculations with multigrid-Newton methods*, Impact Comput. Sci. Engrg., 5 (1993), pp. 75–110.
[15] M. LEE AND F. A. MILNER, *Mixed finite element methods for nonlinear elliptic problems: the p-version*, Numer. Methods Partial Differential Equations, 12 (1996), pp. 729–741.
[16] A. MASUD AND T. J. R. HUGHES, *A stabilized mixed finite element method for Darcy flow*, Comput. Methods Appl. Mech. Engrg., 191 (2002), pp. 4341–4370.

ETNA
Kent State University and
Johann Radon Institute (RICAM)

[17] F. A. MILNER AND E. J. PARK, *A mixed finite element method for a strongly nonlinear second order elliptic problem*, Math. Comp., 64 (1995), pp. 973–988.
[18] E. J. PARK, *Mixed finite element methods for nonlinear second order elliptic problems*, SIAM J. Numer. Anal., 32 (1995), pp. 865–885.
[19] J. E. ROBERTS AND J.-M. THOMAS, *Mixed and hybrid methods*, in Handbook of Numerical Analysis vol. II, P. G. Ciarlet and J. L. Lions, eds., North-Holland, Amsterdam, 1991, pp. 523–639.
[20] R. VERFÜRTH, *A posteriori error estimates for nonlinear problems. Finite element discretizations of elliptic equations*, Math. Comp., 62 (1994), pp. 445–475.
[21] ———, *A Review of a Posteriori Error Estimation and Adaptive Mesh-Refinement Techniques*, Wiley-Teubner, Chichester, 1996.
[22] A. ŽENÍŠEK, *Nonlinear Elliptic and Evolution Problems and Their Finite Element Approximations*, Academic Press, London, 1990.